Deconvolution of global SS precursor data: A novel approach in the analysis of seismic mantle discontinuities

Ask for:
Brechtje Brons
b.brons@uu.nl

Brechtje Brons[1], Douwe van Hinsbergen[1], Arwen Deuss[1] | 1. Department of Earth Sciences, Utrecht University

Introduction

Seismic discontinuities are closely linked to mineralogical phase transitions and convection processes within the Earth's mantle. Thus, accurately mapping the discontinuities and their spatial variations in sharpness, depth, and topography is key to understanding the thermal and chemical evolution of the Earth's mantle and its dynamic behavior. This study aims to improve seismic discontinuity investigation by using **SS precursor observations** and extending existing precursor analysis approaches using a **deconvolution method**.

Findings: The deconvolution method successfully resolves the MTZ thickness and distribution of minor discontinuities. Additionally, this approach provides the possibility to distinguish a robust major phase sidelobe from an actual precursor arrival. Finally, the deconvolution may offer insight into precursor waveform distortions.

Data

We use **SS precursors**, which are underside reflections from seismic mantle discontinuities that arrive prior to the main SS phase due to a shorter path through the mantle (Fig 1.). We collected events with 6 < M_W < 7, for depths < 75 km, and an epicentral distance range of 100º-180º. Our final dataset consists of **~24.000 traces** that have automatically been picked and aligned on the SS phase peak.

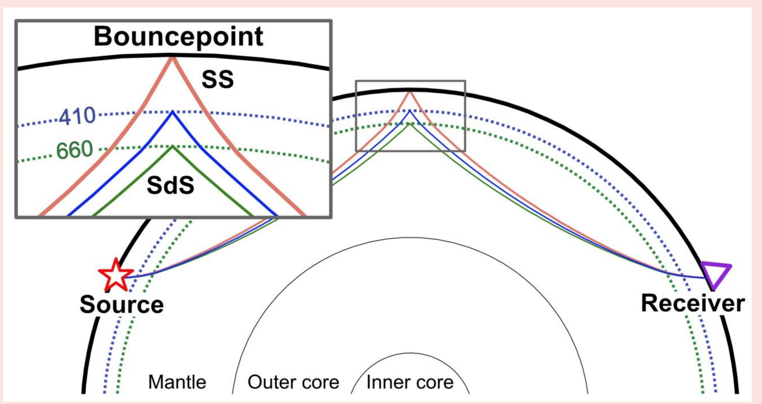

Figure 1: Ray paths of the SS wave (red) and its precursors (SdS), reflecting off the underside of discontinuities at d km depth below the SS bouncepoint. The 410- and 660-km discontinuities are shown in blue and green respectively.

Methods

Deconvolution

Traces are stacked using the **slant stack** method and the robustness of the signal is determined via **bootstrap resampling** (Efron and Tibshirani, 1991). Additionally, we employ an **iterative deconvolution procedure** typically used in receiver function studies (Fig. 2). By combining the bootstrap and deconvolution methods, we can identify and distinguish (minor) precursor phases from robust sidelobes of major SdS phases (Fig. 3) and observe global mantle discontinuities (Fig. 4).

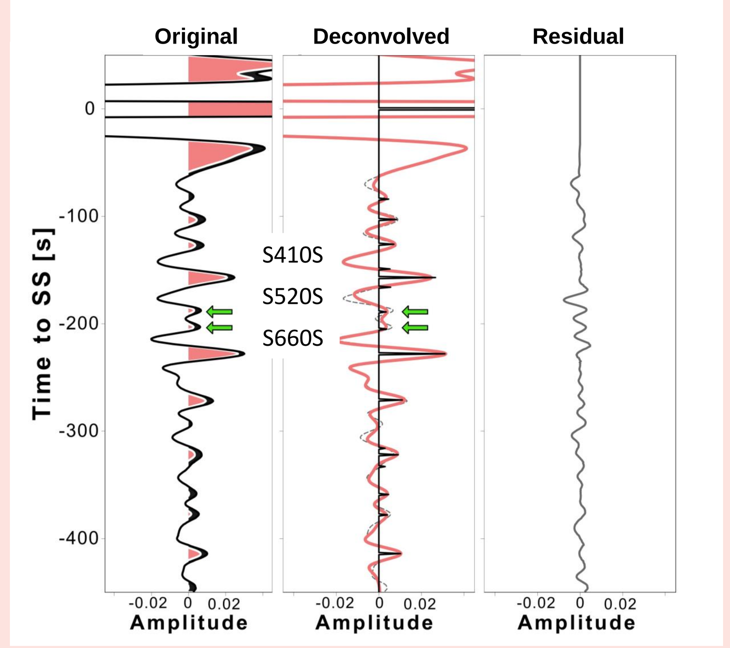

Figure 3: Example of the deconvolution method, showing the original bootstrapped stack (left), with robust peaks in red, the deconvolved stack (middle), and the residual trace (right). The green arrows indicate a splitted S520S for both the bootstrapped and the deconvolved stacks, suggesting that the splitting is not related to the S410S and S660S sidelobes.

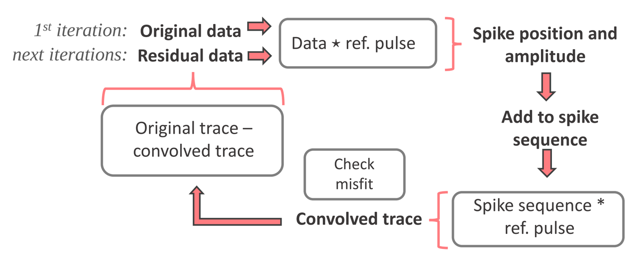

Figure 2: Schematic visualization of the iterative deconvolution procedure.

Waveform analyses

In many deconvolved traces we find smaller amplitude spikes around the major SdS spikes (Fig. 5), indicating a slight waveform distortion of the SdS phases compared to the reference SS phase. This observation may provide unique possibilities for **future SS and SdS waveform analyses**.

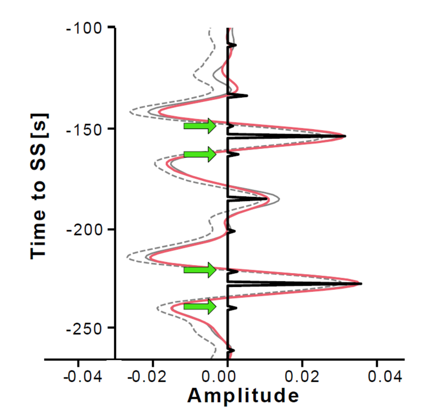

Figure 5: Deconvolved trace with smaller amplitude spikes (green arrows) around major phase spikes.

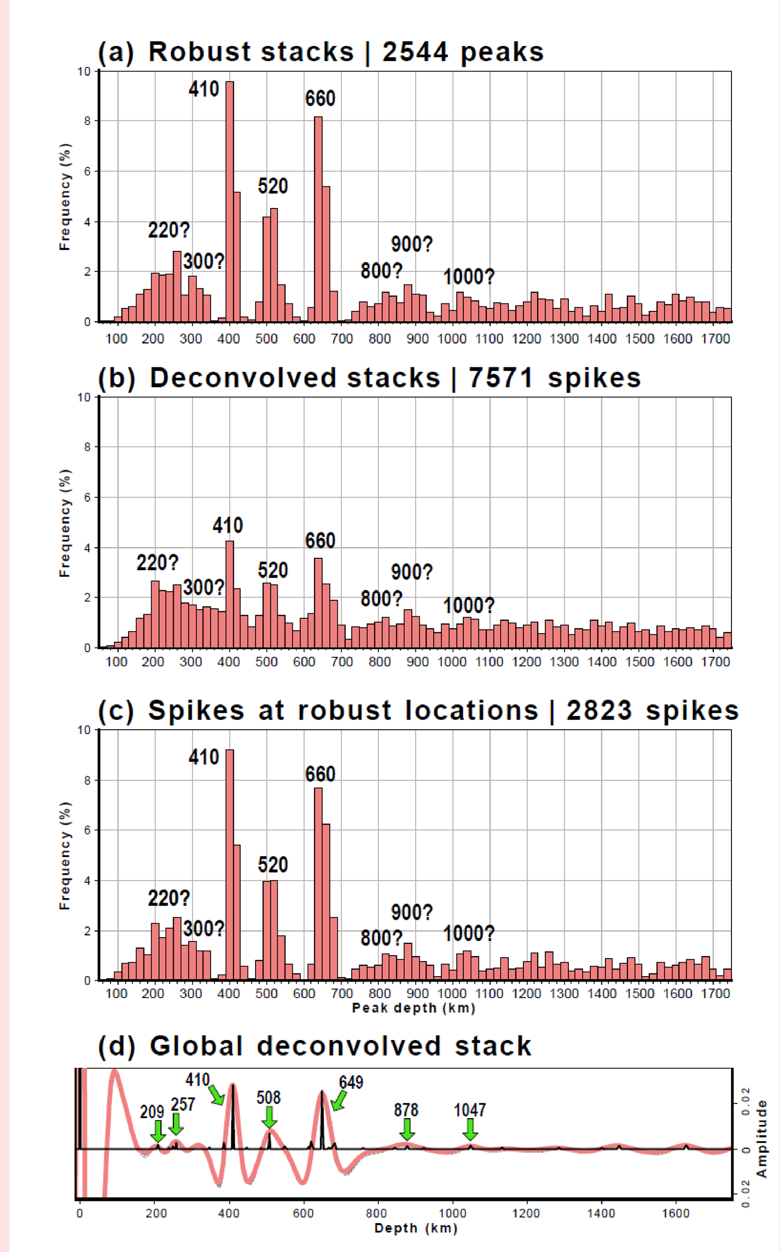

Figure 4: Histograms showing the depth distribution of the (a) Robust data set (from bootstrapping), (b) Deconvolved data set, and (c) Filtered deconvolved data set that only contains the spikes at robust data intervals. (d) depicts the deconvolved global stack of all data.

Results and Interpretations

520-km and 560-km discontinuity

The deconvolved data is used to analyze and **visualize seismic mantle discontinuities**, including the 520- and 560-km discontinuities (Fig. 6a). We observe splitting of the 520-km discontinuity (i.e., two separate reflections at ~520 and ~560 km depth; Fig. 6b; Fig. 7) at significantly less locations than other precursor studies (Deuss and Woodhouse, 2001; Tian et al., 2020).

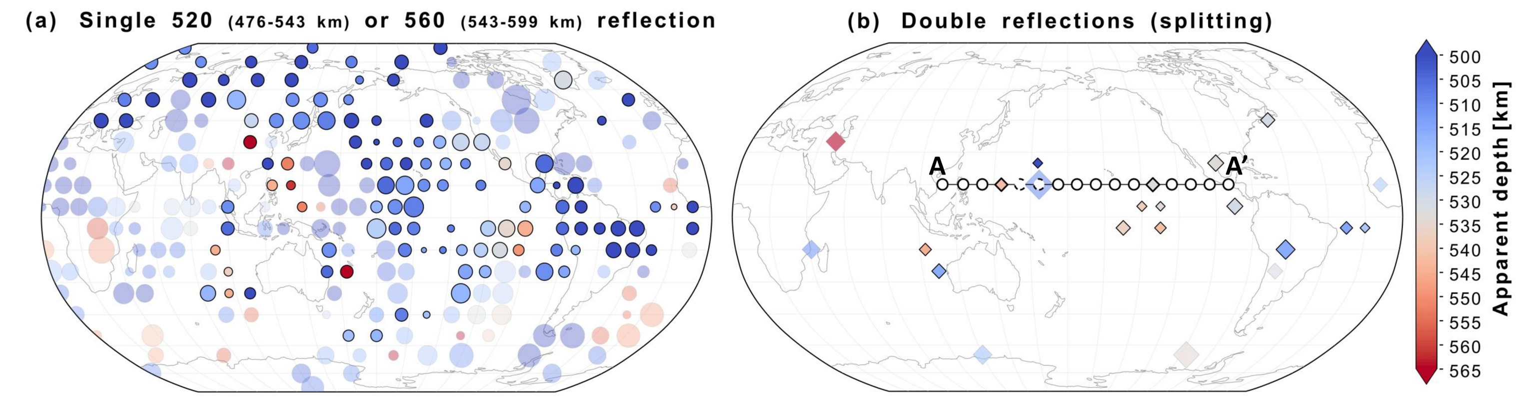

Figure 6: Global maps of (a) the 520 km and 560 km discontinuities, and (b) double reflections referred to as splitting. A-A' indicates the cross-section through the Pacific Ocean (Fig. 7).

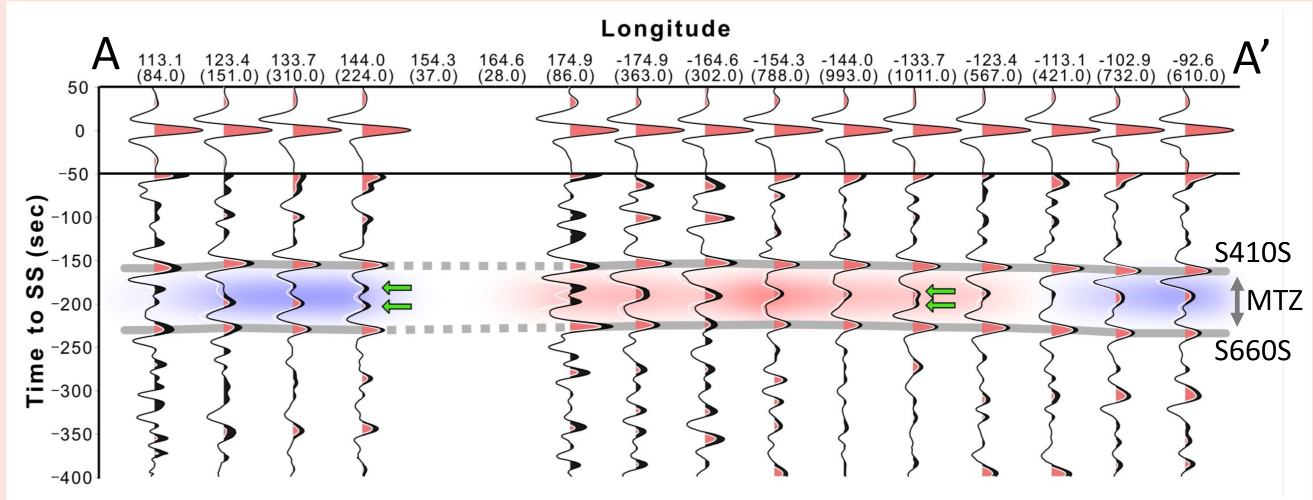

Figure 7: MTZ thickness along a cross section through the Pacific Ocean. Red shading denotes a thinner thickness than average (241.4) and blue shading represents a thicker than average MTZ. The green arrows show two caps with a splitted 520 km discontinuity.

Mantle Transition Zone

We also analyze the 410- and 660-km discontinuities which bound the mantle transition zone (MTZ). Similar to other studies (Deuss, 2009; Waszek et al., 2021), we observe a **thickened MTZ** surrounding the Pacific Ocean (Fig. 8), showing that the deconvolution successfully identifies SS precursor arrivals.

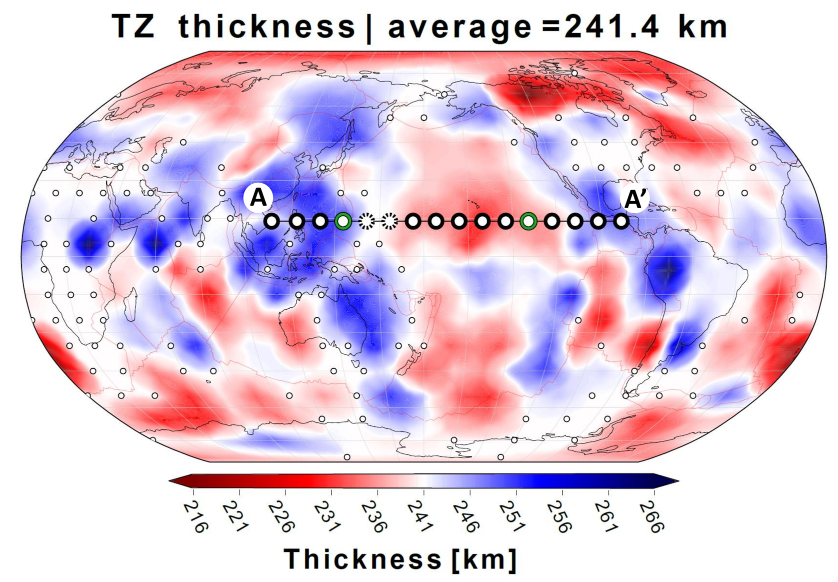

Figure 8: Global map of the MTZ thickness. Green circles along A-A' indicate locations where we find a splitted 520-km discontinuity (Fig. 6, 7)

Conclusions

- Precursor arrivals can be identified and distinguished from robust sidelobes by combining the bootstrap method and the deconvolution method.
- We observe splitting of the 520-km discontinuity using the deconvolution method.
- We find a thickened MTZ around the Pacific Ocean.
- Deconvolution has the potential to contribute to (future) waveform analyses.

REFERENCES:
Deuss, A., & Woodhouse, J. (2001). Seismic observations of splitting of the mid-transition zone discontinuity in Earth's mantle. *Science*, *294*(5541), 354-357.
Deuss, A. (2009). Global observations of mantle discontinuities using SS and PP precursors. *Surveys in geophysics*, *30*, 301-326.
Tian, D., Lv, M., Wei, S. S., Dorfman, S. M., & Shearer, P. M. (2020). Global variations of Earth's 520-and 560-km discontinuities. *Earth and Planetary Science Letters*, *552*, 116600.
Tibshirani, R. J., & Efron, B. (1993). An introduction to the bootstrap. *Monographs on statistics and applied probability*, *57*(1).
Waszek, L., Tauzin, B., Schmerr, N. C., Ballmer, M. D., & Afonso, J. C. (2021). A poorly mixed mantle transition zone and its thermal state inferred from seismic waves. *Nature Geoscience*, *14*(12), 949-955.